Journal of Alloys and Compounds 489 (2010) 275–280

Contents lists available at ScienceDirect

Journal of Alloys and Compounds

journal homepage: www.elsevier.com/locate/jallcom

Effect of chamber pressure and hydrogen on the formation of C_3N_4 films deposited on quartz substrates via MPCVD

Yu-Shiang Wu*, Sih-Wei Wu

Department of Mechanical Engineering, China University of Science and Technology, Taipei 115, Taiwan

ARTICLE INFO

Article history:
Received 11 August 2009
Received in revised form
13 September 2009
Accepted 15 September 2009
Available online 23 September 2009

Keywords:
Nitride materials
Vapor deposition
Microstructure
X-ray diffraction
AFM

ABSTRACT

Carbon nitride (C_3N_4) films were deposited on quartz substrates via microwave plasma chemical vapor deposition. C_3N_4 films were synthesized under different chamber pressures with and without hydrogen. X-ray diffraction (XRD) revealed films with better α-C_3N_4 and β-C_3N_4 structures above 90 Torr chamber pressure with hydrogen condition. When the chamber pressure increases, the C_3N_4 crystal phase is stronger and more conspicuous. Scanning electron microscopy (SEM) shows the surface morphology of C_3N_4 films exhibiting the hexagonal rod structure. Low chamber pressure resulted in small grains, while higher pressures resulted in large grains. The C_3N_4 grains were about 10–12 μm in length and 6–8 μm in width under 100 Torr chamber pressure and hydrogen condition. The center line average roughness from atomic force microscopy (AFM) images showed that the average roughness with hydrogen was higher than that without hydrogen. Fourier transform infrared (FT-IR) spectroscopy confirmed that all the C_3N_4 films contained C–N bonds. The hardness of C_3N_4 films measured using a nanoindenter with hydrogen condition was higher than that without hydrogen.

1. Introduction

Following the structure of β-Si_3N_4, Liu and Cohen [1,2] replaced Si with C and presented a theoretical calculation to predict β-C_3N_4 hardness, which was favorably compared with diamond. Diamond is the hardest known material with a hardness of 100 GPa; second to it is BN with a hardness of 50 GPa [3]. Hardness is a significant property in practical applications as it effects the elastic and plastic deformation and ability to destroy the material. It also describes the residual deformation against destruction. Zhao and Fan [4] used first-principles calculations to show that carbon nitride (C_3N_4) has five structures: α-C_3N_4, β-C_3N_4, cubic-C_3N_4, cubic spinel-C_3N_4, and defect zinc-blende-C_3N_4. C_3N_4 is a new material that does not exist in nature. It has excellent mechanical and physical properties such as high hardness, low friction coefficient, wide energy band gap, and non-poisonous, which make it suitable for application in mechanical, photoelectron, and biomedical engineering as well as the military.

Several researchers have attempted to synthesize C_3N_4 film as a super hardness material using different methods. Chemical vapor deposition (CVD) [5–15] and physical vapor deposition (PVD) [16–21] were more successful than other methods. CVD methods include microwave plasma chemical vapor deposition (MPCVD) [5–13], hot-wire chemical vapor deposition (HWCVD) [14], and synchrotron radiation assisted chemical vapor deposition (SRCVD) [15], while PVD methods include RF magnetron sputtering [16], DC magnetron sputtering [17–19], glow discharge [20], dual ion beam sputtering [21], and ion beam assisted deposition (IBAD) [22]. However, the hardness of the film fabricated using those methods is still far from expectation. Further adjustments to the process parameters and substrates need to be done to synthesize high hardness C_3N_4 films. Previous MPCVD methods have used Si as the deposition substrate for the fabrication [5–10]. Metal substrates such as Pt [10,11], Ni [12], Ta [13], and Mo [13] have also been used. MPCVD generates high N atom flow and synthesize C_3N_4 films with more success. For chamber pressures of 20–50 Torr, the surface morphology exhibited hexagonal rods. The grain size was small: about 1.5–2 μm in length and 0.5 μm in width, and irregular grain surface was also observed.

In this study, C_3N_4 films were synthesized with a quartz substrate for the first time via MPCVD under different chamber pressures (60–100 Torr). Large and clear hexagonal rod crystal grains were synthesized at high chamber pressures, and strong C_3N_4 diffraction peaks were observed with main C–N bonds. The phase structure of C_3N_4 films was analyzed by X-ray diffraction (XRD). The surface morphology and surface roughness were investigated by scanning electron microscopy (SEM) and atomic force microscopy (AFM). The bonds of the C_3N_4 films were character-

* Corresponding author at: 245, Sec. 3, Yen-Chiu-Yuan Road, Nankang, Taipei 115, Taiwan. Tel.: +886 2 27867048x37; fax: +886 2 27867253.
E-mail address: yswu@cc.cust.edu.tw (Y.-S. Wu).

0925-8388/$ – see front matter.
doi:10.1016/j.jallcom.2009.09.070

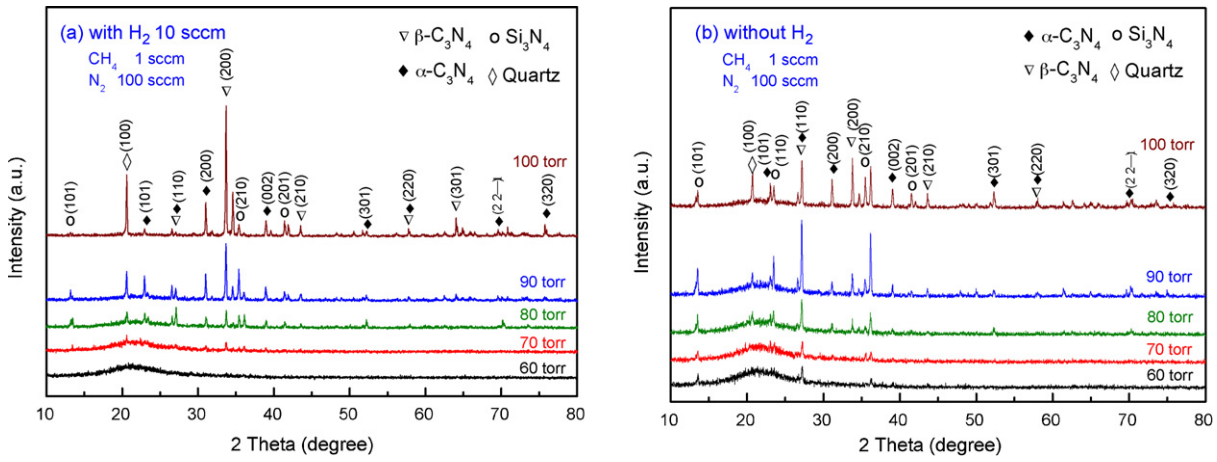

Fig. 1. XRD patterns of C_3N_4 films under different chamber pressures: (a) with hydrogen and (b) without hydrogen.

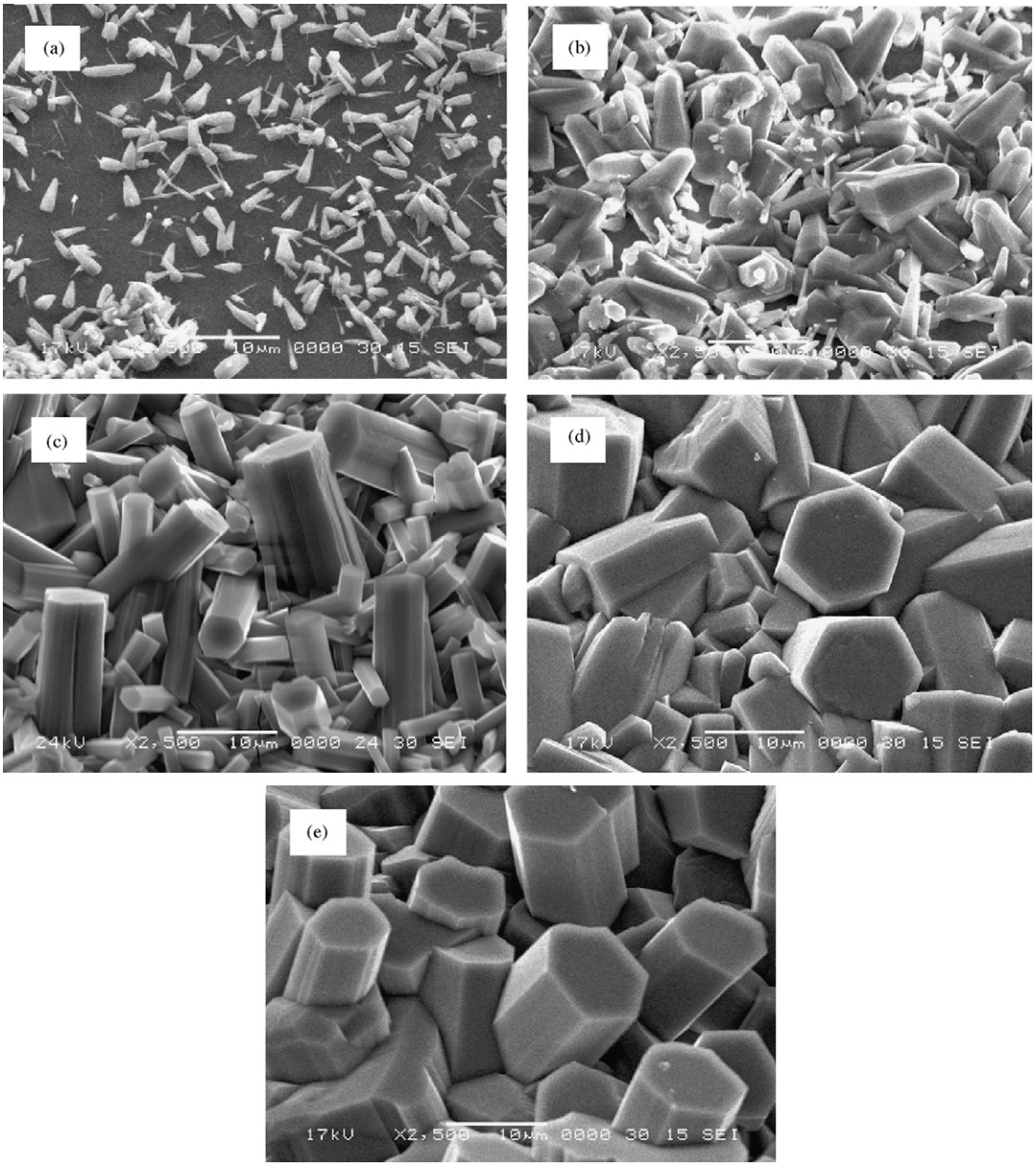

Fig. 2. SEM images of C_3N_4 films with hydrogen condition under different chamber pressures: (a) 60 Torr, (b) 70 Torr, (c) 80 Torr, (d) 90 Torr, and (e) 100 Torr.

ized by Fourier transform infrared (FT-IR) and the hardness was measured using a nanoindenter.

2. Experimental procedure

The C_3N_4 films were deposited with a MPCVD equipment system (ITRI, MP2000-DH2). The apparatus is equipped with a maximum microwave power of 2 kW and 2450 ± 50 MHz microwave frequency. Gas mixtures of hydrogen (H_2, 99.999%), methane (CH_4, 99.95%), and nitrogen (N_2, 99.999%) were used as precursors. A vacuum was created below 7×10^{-3} Torr through a turbomolecular pump and a rotary pump. Two different parameters were used as experiment variables: with and without hydrogen condition. The flow rates were controlled by mass flow controllers of precursors as 1 sccm for CH_4, 100 sccm for N_2, and 0 sccm (without hydrogen)/10 sccm (with hydrogen) for H_2. The microwave power was kept at 1.2 kW under different chamber pressures of 60, 70, 80, 90, and 100 Torr. The deposition time was 4 h. Quartz was used as the deposition substrate in this work. A quartz sheet (1 mm thick) was selected as the substrate material, and was cut in 15 mm × 15 mm pieces of 0.7 mm thickness. Prior to MPCVD, an ultrasonic polishing technique was first applied for 8 h to all substrates using diamond paste (mean particle size 6 μm). The substrates were then washed using a standard cleaning chemical with acetone and deionized (DI) water for 20 min, and were cleaned using pure hydrogen plasma at 1 kW for 20 min before deposition.

The phase of C_3N_4 films was analyzed by XRD (Shimadzu XRD-6000) with a 2θ range of 10–85°, a step size of 0.05°, and a step time of 2 s. The surface morphology and roughness of C_3N_4 films were investigated by SEM (Jeol JSM-5600) and AFM (Seiko NPX110), respectively. The bonds of C_3N_4 films were characterized by FT-IR (Horiba FT-730) and the hardness was measured using a nanoindenter (Psia, XE-100 Hysitron TriboScopeR).

3. Results and discussion

Fig. 1(a) shows XRD patterns of C_3N_4 films deposited on quartz substrates with hydrogen under different chamber pressures. At 60 Torr, there are no clear diffraction peaks, and only amorphous quartz substrate (SiO_2) diffraction is observed. When the cham-

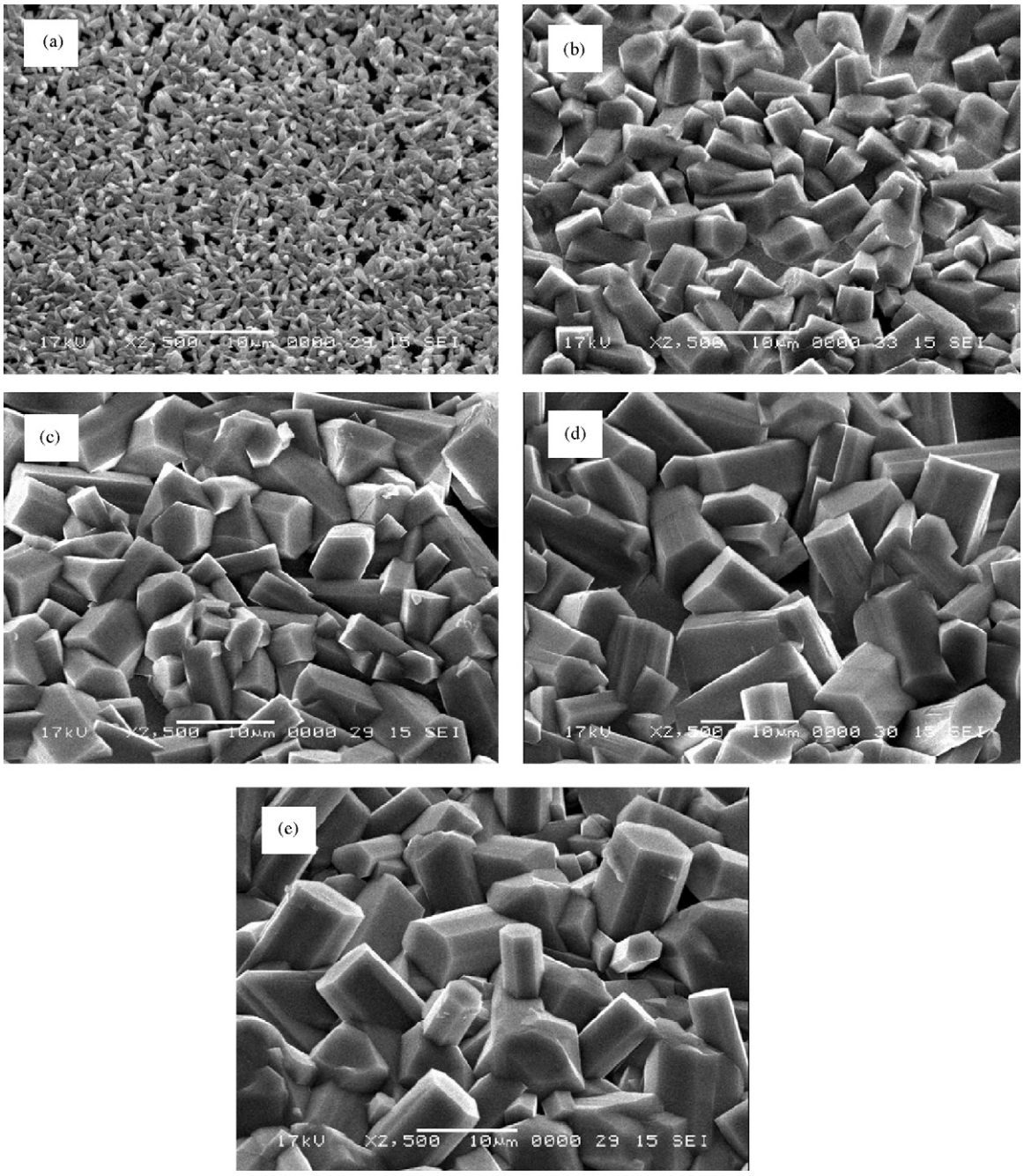

Fig. 3. SEM images of C_3N_4 films without hydrogen condition under different chamber pressures: (a) 60 Torr, (b) 70 Torr, (c) 80 Torr, (d) 90 Torr, and (e) 100 Torr.

ber pressure was increased to 70 and 80 Torr, the crystal structure started to exhibit clear diffraction peaks. When the pressure was further increased to 90 and 100 Torr, strong β-C_3N_4 diffraction peaks (2 0 0) were observed at 33°. Thus, the higher the chamber pressure, the stronger was the diffraction peak, as higher pressures enhanced the density of the plasma sphere. The higher density dissociated the precursors and increased the crystal growth of the films. Fig. 1(b) shows the XRD patterns of C_3N_4 films deposited on quartz substrates without hydrogen condition. The crystal structures of α-C_3N_4 and β-C_3N_4 were present above 90 Torr under both conditions of with and without hydrogen. However, the major diffraction peak at 33° without hydrogen condition was lower than that with hydrogen because there was no hydrogen as the precursor to dissociation. XRD patterns revealed films with better α-C_3N_4 and β-C_3N_4 structures above 90 Torr chamber pressure with hydrogen condition. Some α-C_3N_4 and β-C_3N_4 diffraction peaks appeared to overlap, and some diffraction peaks of Si_3N_4 were exhibited as the N atoms reacted with the quartz substrate.

Fig. 2(a)–(e) shows the SEM images of C_3N_4 films with hydrogen for different chamber pressures. The grains at 60 Torr chamber pressure were small and dispersed, with a length of ~2 μm and a width of ~1 μm (Fig. 2(a)). At 70 Torr, the grain size was larger, but the grains were not of uniform size, and the distribution was more uniform (Fig. 2(b)). As the pressure was increased, the grain clearly transformed to a hexagonal rod (Fig. 2(c)). At 90 and 100 Torr, the grains transformed into complete hexagonal rods of length 10–12 μm and width 6–8 μm, and the grains were dispersed evenly, indicating non-directional growth (Fig. 2(d) and (e)). Fig. 3(a)–(e) shows the SEM images of C_3N_4 films without hydrogen condition for different chamber pressures. At 60 Torr, the grains of length ~1 μm and width ~0.5 μm were irregular. At 70, 80, 90, and 100 Torr, the grain transformed gradually and turned into complete hexagonal rods. The grains were dispersed evenly, indicating non-directional growth. The SEM images showed that the grain size increased with chamber pressure because high pressures result in an improvement in the density of the plasma sphere. That is, when the chamber pressure was low, the crystallization was weak, and when it was high, the crystallization was strong. This enhanced crystallization led to the formation of complete hexagonal rods.

Fig. 4(a) and (b) shows the AFM images of C_3N_4 films with hydrogen under 60 and 100 Torr chamber pressures. We found that different chamber pressures cause different grain sizes: the higher the pressure, the larger are the grain size and film thickness. Fig. 4(c) and (d) shows the AFM images of C_3N_4 films without hydrogen condition under 60 and 100 Torr. The growth situation was as the same as that with hydrogen: the grain size increased with the chamber pressure. AFM results indicated that the hydrogen could enhance the ability of crystal growth. The center line average roughness of C_3N_4 films is shown in Fig. 5. It was calculated by AFM images analysis software. In the with hydrogen case, the average roughness increased with chamber pressure. The average roughness with hydrogen was higher than that without hydrogen because hydrogen promotes the grain growth, and large grains in turn result in a higher roughness. The chamber pressure and hydrogen not only affected the grain size, but also enhanced the average roughness.

Fig. 6(a) shows the FT-IR spectra with hydrogen under different chamber pressures. The results indicated that the C–N bonds increased with the chamber pressure, and also supported the formation of C–N bonds in the α-C_3N_4 and β-C_3N_4 mixtures. C=N and C≡N bonds were not apparent. In theory, C_3N_4 films are composed

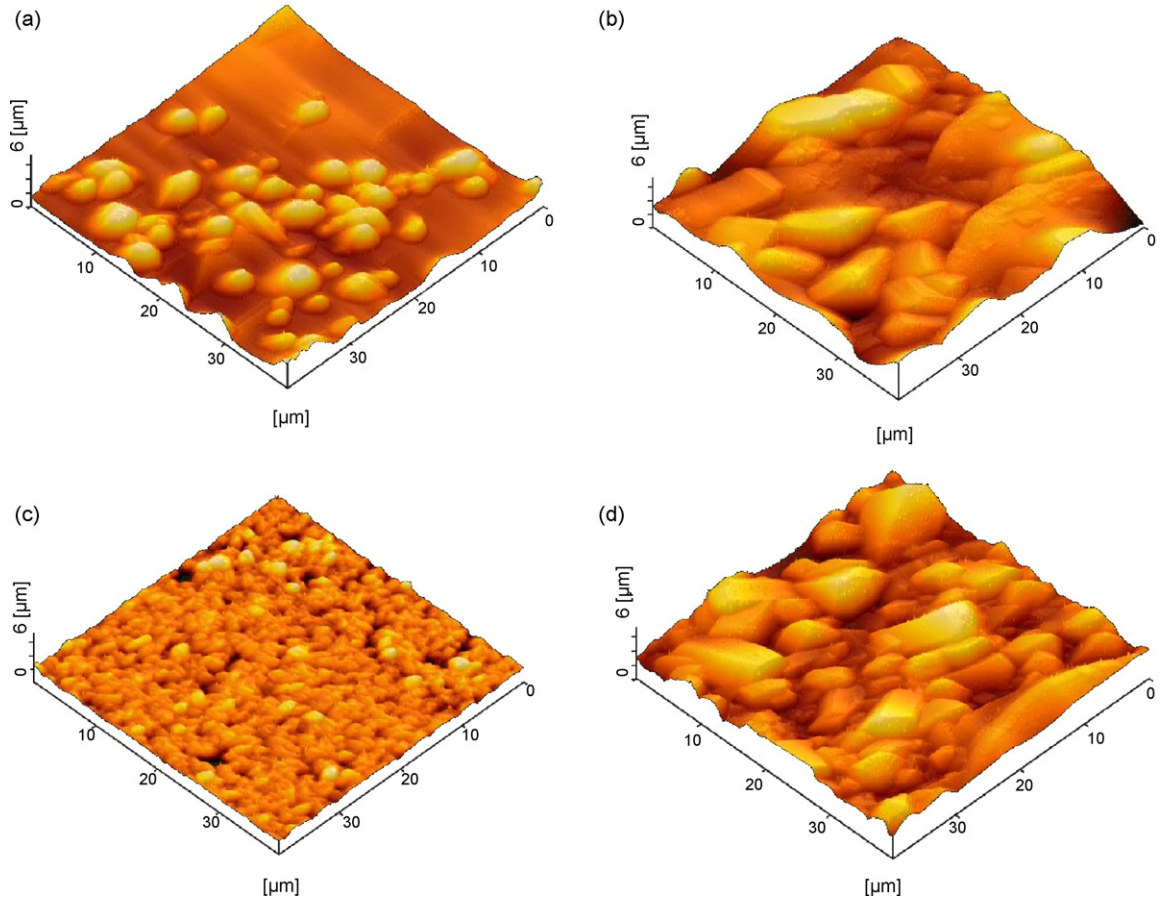

Fig. 4. AFM images of C_3N_4 films with and without hydrogen condition under different chamber pressures: (a) with H_2, 60 Torr; (b) with H_2, 100 Torr; (c) without H_2, 60 Torr; (d) without H_2, 100 Torr.

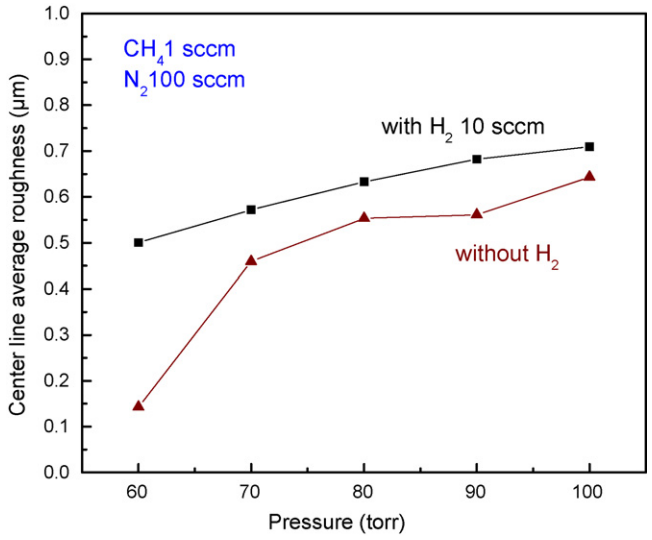

Fig. 5. Center line average roughness of C_3N_4 films under different chamber pressures with hydrogen and without hydrogen condition.

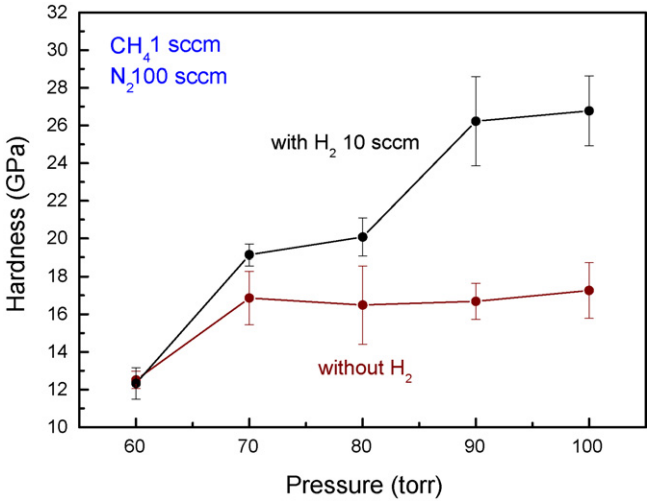

Fig. 7. Hardness of C_3N_4 films under different chamber pressures with and without hydrogen condition.

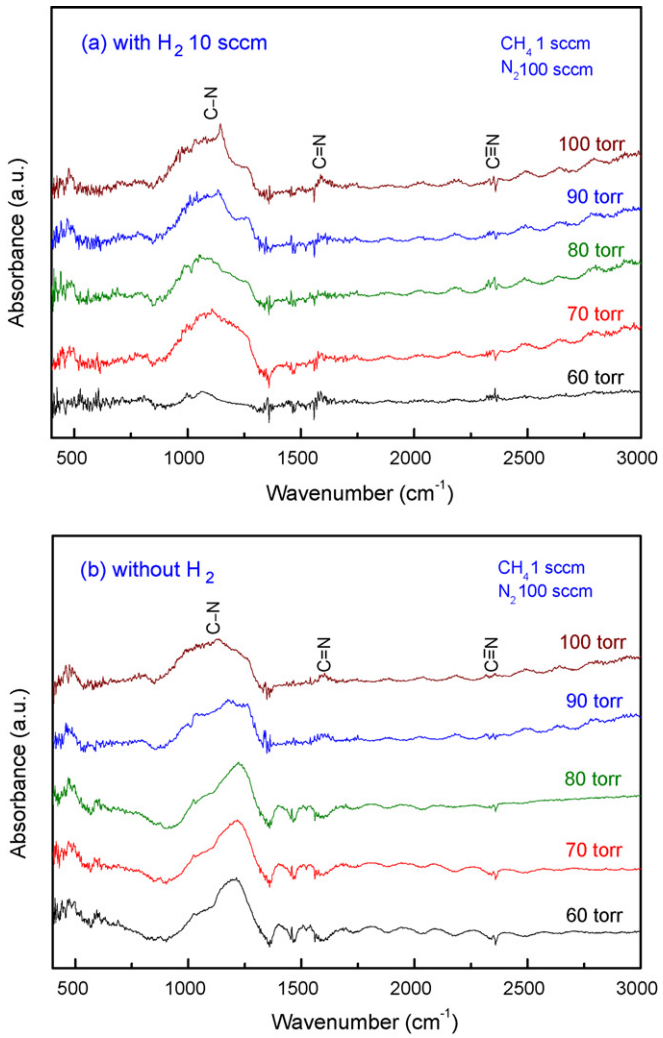

Fig. 6. FT-IR spectra of C_3N_4 films under different chamber pressures: (a) with hydrogen and (b) without hydrogen.

of C–N bonds. The bond length of C_3N_4 C–N bonds, 1.47 Å, is shorter than that of diamond C–C bonds, 1.54 Å. The short bond length exhibited strong bond strength and stability and exhibited excellent properties. Therefore, the deposited films contained a strong C_3N_4 structure from FT-IR analysis. Fig. 6(b) shows the FT-IR spectra of without hydrogen under different chamber pressures of 60, 70, and 80 Torr; the C–N bonds were not obvious. When the chamber pressure increased to 90 and 100 Torr, the C_3N_4 films started to transform the completed C–N bonds. The C=N and C≡N bonds were still not distinct. High chamber pressures caused crystalline C_3N_4 films to form completed C–N bonds, but C=N and C≡N bonds did not increase with chamber pressure. The results show that the chamber pressure influences the C–N bond formation.

According to the hardness analysis of C_3N_4 films (Fig. 7), the hardness increased with the chamber pressure. It increased obviously when the chamber pressure increased from 60 to 70 Torr. According to SEM images, the grain size became large when the chamber pressure rose from 60 to 70 Torr. According to XRD analysis, high chamber pressure results in complete crystal phase. FT-IR spectra present films containing C–N bonds under high chamber pressure. Thus, the properties and hardness improve as the chamber pressure is increased. However, at 90 Torr, the hardness tended to slow down. The relationship of the chamber pressure of C_3N_4 films without hydrogen was similar to that with hydrogen. The maximum hardness of the C_3N_4 films deposited at 100 Torr with hydrogen was 27 GPa. The hardness increased with the chamber pressure, but the hardness without hydrogen was lower than with hydrogen. The AFM images also showed that the grain size without hydrogen was lower than with hydrogen. Therefore, hydrogen not only enhances the growth of grains but also increases the hardness.

4. Conclusion

C_3N_4 films were deposited on quartz substrates via MPCVD under a fixed N_2, CH_4 flow with different chamber pressures. XRD patterns showed that C_3N_4 films could be obtained as welled α-C_3N_4 and β-C_3N_4 crystal phases at chamber pressures above 90 Torr with hydrogen condition. SEM images showed the surface morphology of C_3N_4 films that exhibited hexagonal rod structure. When the chamber pressure increased, the grain size became large; that is, the chamber pressure in combination with hydrogen enhanced the grain size. FT-IR spectra showed that there were C–N bonds in C_3N_4 films. From nanoindenter measurement, we found that the hardness of C_3N_4 films with hydrogen condition was higher than

that without hydrogen. The hardness increased with the chamber pressure, and tended to slow down above 90 Torr. The maximum hardness of the C_3N_4 films was 27 GPa at chamber pressure of 100 Torr with hydrogen. Because there is no hydrogen to enhance the reaction in the without hydrogen condition, the crystal phase, grain size, and hardness of C_3N_4 films were lower than those with hydrogen condition.

Acknowledgements

The authors are thankful for the financial support of National Science Council of Taiwan ROC under grant No. NSC 97-2511-S-157-001.

References

[1] M.L. Cohen, Phys. Rev. B 32 (1985) 7988.
[2] A.Y. Liu, M.L. Cohen, Science 245 (1989) 841.
[3] J.P. Rivière, D. Texier, J. Delafond, M. Jaouen, E.L. Mathé, J. Chaumont, Mater. Lett. 61 (2007) 2855.
[4] J. Zhao, C. Fan, Physica B 403 (2008) 1956.
[5] Y. Sakamot, M. Takaya, Thin Solid Films 475 (2005) 198.
[6] M.N. Uddin, O.A. Fouadb, M. Yamazato, M. Nagano, Appl. Surf. Sci. 240 (2005) 120.
[7] M.N. Uddin, H. Notomi, T. Kida, M. Yamazato, M. Nagano, Thin Solid Films 464–465 (2004) 170.
[8] Y.P. Zhang, Y.S. Gu, X.R. Chang, Z.Z. Tian, D.X. Shi, X.F. Zhang, Mater. Sci. Eng. B 78 (2000) 11.
[9] Y.P. Zhang, Y.S. Gu, X.R. Chang, Z.Z. Tian, D.X. Shi, X.F. Zhang, L. Yuan, Surf. Coat. Technol. 127 (2000) 260.
[10] D.X. Shi, X.F. Zhang, L. Yuan, Y.S. Gu, Y.P. Zhang, Z.J. Duan, X.R. Chang, Z.Z. Tian, N.X. Chen, Appl. Surf. Sci. 148 (1999) 50.
[11] Y.P. Zhang, Y.S. Gu, Mater. Sci. Eng. B 85 (2001) 38.
[12] J. Jiang, W. Cheng, Y. Zhang, M. Lan, H. Zhu, D. Shen, Mater. Lett. 61 (2007) 2243.
[13] Y.S. Gu, Y.P. Zhang, Z.J. Duan, X.R. Chang, Z.Z. Tian, D.X. Shi, L.P. Ma, X.F. Zhang, L. Yuan, Mater. Sci. Eng. A 271 (1999) 206.
[14] S. Mitra, R. Deshpande, T. Hanrath, J. Hartman, Thin Solid Films 430 (2003) 300.
[15] Z. Han, Y. Zhang, Y. Tian, Y. Hu, Y. Kan, X. Zhang, Mater. Sci. Eng. B 78 (2000) 109.
[16] N.A. de Sánchez, C. Carrasco, P. Prieto, Physica B 337 (2003) 318.
[17] J. Xu, X.L. Deng, J.L. Zhang, W. Lu, T. Ma, Thin Solid Films 390 (2001) 107.
[18] M.A. Monclus, A.K.M.S. Chowdhury, D.C. Cameron, R. Barklie, M. Collins, Surf. Coat. Technol. 131 (2000) 488.
[19] Z.H. Huang, B. Yang, C.S. Liu, L.P. Guo, X.J. Fan, D.J. Fu, Mater. Lett. 61 (2007) 3443.
[20] Z.Q. Li, J.Y. Zhou, J. Zhang, T.B. Chen, J. Yuan, J. Alloys Compd. 346 (2002) 230.
[21] J.P. Rivière, D. Texier, J. Delafond, M. Jaouen, E.L. Mathè, J. Chaumont, Mater. Lett. 61 (2007) 2855.
[22] J.X. Yang, F.Z. Cui, I.-S. Lee, Y.P. Jiao, Q.S. Yin, Y. Zhang, Surf. Coat. Technol. 202 (2008) 5737.